Reevaluating electron–phonon coupling strengths: Indium as a test case for *ab initio* and many-body–theory methods

Sven P. Rudin[†], R. Bauer,[‡] Amy Y. Liu,[†] and J. K. Freericks[†]

[†] *Department of Physics, Georgetown University, Washington, D.C. 20057-0995, U.S.A.*

[‡] *Theoretische Physik, Universität Regensburg, D-93040 Regensburg, Germany*

Abstract

Using indium as a test case, we investigate the accuracy of the electron–phonon coupling calculated with state-of-the-art *ab initio* and many-body theory methods. The *ab initio* calculations — where electrons are treated in the local-density approximation, and phonons and the electron–phonon interaction are treated within linear response — predict an electron–phonon spectral function $\alpha^2 F(\omega)$ which translates into a relative tunneling conductance that agrees with experiment to within one part in 10^3. The many-body theory calculations — where $\alpha^2 F(\omega)$ is extracted from tunneling data by means of the McMillan-Rowell tunneling inversion method — provide spectral functions that depend strongly on details of the inversion process. For the the most important moment of $\alpha^2 F(\omega)$, the mass-renormalization parameter λ, we report 0.9±0.1, in contrast to the value 0.805 quoted for nearly three decades in the literature. The *ab initio* calculations also provide the transport electron–phonon spectral function $\alpha_{tr}^2 F(\omega)$, from which we calculate the resistivity as a function of temperature in good agreement with experiment.

I. INTRODUCTION

Materials with phonon-mediated superconductivity were most intensively studied two to three decades ago. In the last decade, especially since the discovery of compounds with high transition temperatures, the experimental study of such low-temperature materials has steadily declined. In contrast, recent years have seen a steady improvement in computational and theoretical methods aimed at describing the electron-phonon coupling in the "old" materials. State-of-the-art *ab initio* methods can now be used to study details of the interaction between electrons and phonons and to estimate transition temperatures. The accuracy of these calculations, in itself worth investigating, also raises the question of how precisely we know the parameters derived from experiments.

The understanding of phonon-mediated superconductivity relies on a detailed description of the coupling between phonons and electrons, most explicit in the electron–phonon spectral function $\alpha^2 F(\omega)$ of Eliashberg theory.[1] The spectral function measures the strength with which phonons scatter electrons on the Fermi surface with an imparted energy ω. With the addition of an effective Coulomb repulsion, i.e., the Morel-Anderson pseudopotential μ^*, $\alpha^2 F(\omega)$ determines all the thermodynamic properties of a phonon-mediated superconductor, including the transition temperature T_C, the critical field, and the specific heat jump at T_C.[2] Rather than treating all scattering events equally, one can also weight each scattering event according to how much the direction of the electronic velocity changes. This weighting results in the *transport* electron–phonon spectral function $\alpha_{tr}^2 F(\omega)$, which determines the transport properties in the normal state.

First-principles density-functional calculations can be used to study the electronic structure, vibrational properties, and electron-phonon coupling in real materials. To calculate quantities such as $\alpha^2 F(\omega)$ and $\alpha_{tr}^2 F(\omega)$, which involve averages over all phonon modes, the density-functional linear-response approach is particularly useful.[3–7] In this approach, the electronic response to atomic displacements is determined self-consistently, and phonon wave vectors throughout the Brillouin zone are accessible without having to construct the large supercells needed in finite-difference-based frozen-phonon or generalized supercell methods.[8–10] This approach has been successfully used to study the electron-phonon interaction and su-

perconductivity in many simple metals that are suitably treated by the approximations inherent in the method, i.e., the local density approximation (LDA) for the electrons and the harmonic approximation for the phonons.[6,7,11]

Alternatively, $\alpha^2 F(\omega)$ and $\alpha_{tr}^2 F(\omega)$ can be extracted from tunneling experiments and optical conductivity data, respectively,[12,13] using the Migdal-Eliashberg theory of superconductivity. In particular for $\alpha^2 F(\omega)$, structure in the tunneling conductance measured across metal-insulator-superconductor junctions reflects structure in the superconducting gap function $\Delta(E)$ resulting from the interaction of the electrons with the phonons.[14,15] In the McMillan-Rowell tunneling inversion method,[12] the Eliashberg equations are solved iteratively to find an $\alpha^2 F(\omega)$ that is consistent with the measured tunneling spectrum. In recent years, improved computational strategies for solving the Eliashberg equations have been developed, allowing for more accurate extractions of $\alpha^2 F(\omega)$ from tunneling data.[16]

In this contribution, we focus on $\alpha^2 F(\omega)$ determined from *ab initio* and many-body theory methods to investigate the accuracy with which electron–phonon parameters are known. The moments of $\alpha^2 F(\omega)$, e.g., the electron–phonon mass-renormalization parameter λ, are quoted for many materials with several digits. Our results show that this is misleading, since for indium we find that λ can only be given to within approximately 10%.

Indium is an ideal candidate for our discussion because high-quality tunneling data are available. It is possible to fabricate clean tunnel junctions and the electron-phonon coupling strength appears large enough to yield a good signal-to-noise ratio.[17,18] From the theoretical point of view, indium also serves as a good test case, since it is a relatively simple metal in which relativistic effects are small. The core–valence interaction can be accurately treated with a pseudopotential, and since there are only s and p valence electrons, the electronic wave functions can be expanded efficiently in plane waves. Furthermore, our results indicate that the structural and electronic properties of indium are well described by the LDA and that anharmonic effects are small at temperatures near or below the Debye temperature.

Structure of this paper. The first-principles and many-body theory calculations are outlined in Section II. We refer readers to the references for discussions of the many finer, technical points not included here. We present and discuss the results of our calculations in Section III, and give concluding remarks in Section IV.

II. OUTLINE OF THE CALCULATIONS

The *ab initio* procedure consists of three parts: the electronic structure, the vibrational properties, and the electron–phonon coupling.

The electronic structure is calculated in the local density approximation (LDA) of density functional theory, by solving the Kohn-Sham equations self-consistently using the Perdew-Zunger parameterization of the correlation energy.[19] Since it is primarily the valence electrons that determine the structure and hence interact with the phonons, the core electrons are eliminated from the calculation by using a pseudopotential, which is generated by the improved Troullier and Martins scheme.[20] The nonlinearity of the exchange and correlation interaction between the core and valence charge densities is handled with partial core corrections.[21] The Kohn-Sham orbitals are expanded in plane waves with a kinetic energy cutoff of 20 Ry.

Integrations over the Brillouin zone are approximated by sums over discrete sets of $\mathbf{k}$-points. The Kohn-Sham orbitals are calculated for 1056 $\mathbf{k}$-points in the irreducible Brillouin zone (IBZ). These points, generated with the Monkhorst-Pack scheme,[22] originate from a mesh of 24^3 $\mathbf{k}$-points in the full Brillouin zone. To accelerate convergence for this metallic system, we use first-order Hermite-Gaussian smearing with a width of 0.04 Ry.[23] The electronic density of states, in particular the density of states at the Fermi level, $N(E_F)$, is calculated more accurately using the linear tetrahedron method.[24]

The vibrational properties are determined by calculating the self-consistent first-order change in the electron density with respect to atomic displacements.[4] For each phonon wave vector $\mathbf{q}$, this change is used to calculate the dynamical matrix, which in turn is diagonalized to give the phonon eigenvectors $\mathbf{e}_{\mathbf{q}\nu}$ and frequencies $\omega_{\mathbf{q}\nu}$ (ν is a branch label).

Because the linear-response calculation is the most time-consuming step in the *ab initio* procedure, we calculate the phonons for a relatively small set of 59 $\mathbf{q}$-points in the IBZ. The dynamical matrices are obtained on a finer mesh of $\mathbf{q}$-points by a Fourier deconvolution, where the calculated dynamical matrices are Fourier-transformed to obtain the real-space force constants, which can then be used to form the dynamical matrix at arbitrary $\mathbf{q}$-points. The phonon dispersion in the vicinity of $\mathbf{q}$=0 is found to be sensitive to the number of

atomic shells included in the force constant model. To ensure the accuracy of the long-range force constants, we also do the full linear-response calculation for several small $\mathbf{q}$-points not in our original mesh of 59 points.

The final *ab initio* step is to calculate the coupling of each phonon to the electron states. A phonon $\mathbf{q}\nu$ will scatter an electron from a state $|n\mathbf{k}\rangle$ to a new state $|n'\mathbf{k}'\rangle$ with a strength determined by the resulting first-order change $\delta V_{\mathbf{q}}^{SCF}$ in the self-consistent potential. For atoms of mass M, the electron–phonon matrix elements are given by

$$g(n\mathbf{k}, n'\mathbf{k}', \nu\mathbf{q}) = \sqrt{\frac{\hbar}{2M\omega_{\mathbf{q}\nu}}} \langle n'\mathbf{k}'|\mathbf{e}_{\mathbf{q}\nu} \cdot \delta V_{\mathbf{q}}^{\mathbf{SCF}}|n\mathbf{k}\rangle, \qquad (1)$$

with the restriction $\mathbf{k}' = \mathbf{k} + \mathbf{q}$. Since only electrons near the Fermi surface can scatter via phonons, the average coupling of electrons to a phonon $\mathbf{q}\nu$ is expressed in the doubly-constrained Fermi surface average, $\langle\langle|g_{\mathbf{q}\nu}|^2\rangle\rangle$.[8] As with the dynamical matrices, the electron–phonon matrices are calculated on the coarse mesh of 59 $\mathbf{q}$-points and then interpolated to a denser mesh by means of a Fourier deconvolution. The electron–phonon spectral function, which involves coupling to all phonons, is given by[25]

$$\alpha^2 F(\omega) = N(E_F) \sum_{\mathbf{q}\nu} \delta(\hbar\omega - \hbar\omega_{\mathbf{q}\nu})\langle\langle|g_{\mathbf{q}\nu}|^2\rangle\rangle. \qquad (2)$$

In our calculations, the δ function in Eq. (2) is replaced by a Gaussian of width 0.5 meV.

With slight modifications, the above formalism can be used to compute the transport spectral function $\alpha_{tr}^2 F(\omega)$ for the phonon-limited electrical resistivity, $\rho(T)$, where not all scattering events are equally important. For example, forward scattering events do not change the direction of the electron velocity $\mathbf{v}_{n\mathbf{k}}$ and do not contribute to the resistivity. To this end an efficiency factor,[13]

$$\eta_{n\mathbf{k},n'\mathbf{k}'} = 1 - \frac{\mathbf{v}_{n\mathbf{k}} \cdot \mathbf{v}_{n'\mathbf{k}'}}{|\mathbf{v}_{n\mathbf{k}}|^2}, \qquad (3)$$

is used to weight the electron–phonon matrix elements in the calculations of $\alpha_{tr}^2 F(\omega)$. The electrical resistivity is then given by[13,26]

$$\rho(T) = \frac{3\pi\Omega}{e^2 N(E_F)\langle\mathbf{v}^2\rangle} \frac{1}{2k_B T} \int_0^\infty \hbar\omega \frac{\alpha_{tr}^2 F(\omega)}{\sinh^2(\hbar\omega/2k_B T)} d\omega, \qquad (4)$$

with Ω the cell volume and $\langle\mathbf{v}^2\rangle$ the Fermi-surface average of the electron velocity. This is a variational solution to the semiclassical Boltzmann equation in which the Fermi surface is

assumed to undergo a uniform rigid shift in an applied electric field. Here current–current vertex corrections are included via the efficiency factor, but only to lowest order. As written, Eqs. (3) and (4) are appropriate for isotropic and nearly isotropic materials since $\alpha_{tr}^2 F(\omega)$ is averaged over all directions and $\langle v_x^2 \rangle$ is assumed to be equal to $\langle \mathbf{v}^2 \rangle / 3$.

We compare the *ab initio* electron–phonon coupling with experiment both by calculating the tunneling conductance from the *ab initio* $\alpha^2 F(\omega)$ and by extracting the experimental $\alpha^2 F(\omega)$ from tunneling data. The traditional procedure, for which the new computational strategies have been developed, is to calculate the experimental $\alpha^2 F(\omega)$ from tunneling data by solving the Eliashberg gap equations.

The extraction of $\alpha^2 F(\omega)$ from tunneling data is done with the McMillan and Rowell tunneling inversion method.[12] We follow their original prescription: (i) We assume an initial value for $\alpha^2 F(\omega)$ for which (ii) we adjust μ^* to reproduce the experimental superconducting gap at zero temperature Δ_0, which is 0.541 meV for indium; (iii) we compute the functional derivative of the change in the tunneling density of states with respect to a change in the assumed $\alpha^2 F(\omega)$; (iv) we determine the required shift in $\alpha^2 F(\omega)$ to produce the experimental tunneling conductance via a singular-value-decomposition, and (v) we determine the new $\alpha^2 F(\omega)$ by adding a smoothed shift $\delta \alpha^2 F(\omega)$ to it. The new $\alpha^2 F(\omega)$ is then used to begin again with step (ii), and the entire process is repeated until it converges.

While the McMillan–Rowell tunneling inversion procedure is well defined, different computational strategies can be used to solve the Eliashberg equations. We perform the perturbation theory directly on the imaginary-frequency axis with an energy cutoff of six times the maximum phonon frequency, ω_{max} (beyond which $\alpha^2 F(\omega) = 0$), and then perform an exact analytic continuation to the real axis.[16,27] This method treats the Morel-Anderson pseudopotential properly because the sharp cutoff on the imaginary-frequency axis translates into a smooth cutoff when analytically continued to the real axis.[28] In addition, the perturbation theory is performed relative to the exact result in the normal state. These details are necessary to accurately predict a superconducting T_C from the experimental data. The inputs are the experimental tunneling conductance and the superconducting gap at zero temperature. The outputs are the electron–phonon spectral function $\alpha^2 F(\omega)$ and the Morel-Anderson pseudopotential μ^*. The transition temperature T_C is then calculated with

the T-matrix method of Owen and Scalapino,[29] rather than using an approximate equation such as the McMillan formula.

The accuracy of the tunneling experiments suffers at low energy, where the signal near the gap edge shows a large slope, and at high energy, where the detailed structure in $\Delta(E)$ is washed out because it enters the measurement in the form $E^2 - \Delta^2(E)$. The experimental data also depends critically on the precise value of the superconducting gap at zero temperature, Δ_0, because this produces the BCS form for the tunneling conductance; the strong-coupling corrections, which are employed to extract $\alpha^2 F(\omega)$, are the deviations from the BCS form. Hence an $\alpha^2 F(\omega)$ extracted from tunneling data is usually constrained by assuming that it has a quadratic dependence at low energy and that it vanishes beyond a maximal phonon frequency (some researchers include a quadratic dependence at high energies too). Unfortunately, neither the upper limit of the low-energy quadratic behavior, nor the exact value of ω_{max} or the frequency dependence near the ω_{max} is known. In principle, ω_{max} should be chosen to be equal to the maximum bulk phonon frequency, but it frequently is allowed to be somewhat larger to allow for the effects of interface phonons. We adjust the region of quadratic behavior and the maximal phonon frequency in different fitting procedures, and impose a linear form on $\alpha^2 F(\omega)$ to bring it to zero at ω_{max}.

III. RESULTS AND DISCUSSION

The ground-state crystal structure of indium is face-centered tetragonal (fct). As is typical with LDA calculations, we find that compared to experiment the equilibrium volume is approximately 5% too small. The tetragonal lattice parameters are calculated to be a=4.51 Å and c=4.84 Å; the experimental values are a=4.58 Å and c=4.94 Å.[30] The calculated and measured c/a ratios agree to better than 1%. Our linear-response calculations are all performed using the theoretical lattice parameters.

The calculated electronic density of states (DOS) is plotted in Figure 1. The DOS has a free-electron-like behavior at low energies, but develops more structure at higher energies where bands cross the Bragg planes. The dashed curve shows the DOS for a free electron gas with the same average valence-electron density as indium. The two curves differ significantly,

indicating that band-structure and correlation effects within LDA strongly renormalize the electron mass in indium. The DOS at E_F is reduced by about 26% compared to the free electron value. Unfortunately, it is difficult to compare the calculated DOS directly with magnetic susceptibility measurements for indium since these experiments find diamagnetic rather than Pauli paramagnetic behavior at low temperatures.

The inset to Figure 1 shows the DOS near E_F, where the DOS varies only by a few percent on the scale of phonon energies. This is in particular true over the range $E_F \pm 6\omega_{max}$, where we assume a constant electronic DOS for the tunneling inversion.

Figure 2 shows the excellent agreement between the measured and calculated phonon dispersion curves. The experimental data is taken from neutron diffraction, and is reported with an 11th-neighbor, 19-parameter Born–von Kármán fit.[30] Along the direction from Z to X for which no direct experimental data are available, we find good agreement between the fit to the experiment and our calculated phonon dispersion, though the latter shows more structure than the fit. This structure, if real, may be more detailed than can be extracted from the available experimental data.

The electrical resistivity, calculated with Eq. (4), is plotted along with experimental data from polycrystalline samples[31] in Figure 3. Eq. (4) is expected to be most accurate in the temperature range of about $\Theta_D/5 \lesssim T \lesssim 2\Theta_D$, with the Debye temperature $\Theta_D = 129$ K.[32] At very low temperatures anisotropy effects become important, while at high temperatures anharmonic effects must be included.[33] Although the crystal structure of indium is tetragonal, electrical resistivity measurements on single crystals find nearly the same results along the a and c directions. This isotropy also appears in our calculations, where $\langle v_x^2 \rangle$ and $\langle v_z^2 \rangle$ differ by less than 5%.

The dashed curve in Figure 3 is calculated using $\alpha^2 F(\omega)$, which is often used as an approximation to $\alpha_{tr}^2 F(\omega)$. The rough agreement between the dashed curve and the measured resistivity justifies the approximation in cases when $\alpha_{tr}^2 F(\omega)$ is not known. However, including the correct weighting with the efficiency factor $\eta_{n\mathbf{k},n'\mathbf{k}'}$ brings the calculated resistivity into much better agreement with experiment for temperatures up to well above the Debye temperature. The transport electron-phonon coupling parameter λ_{tr} is found to be 0.74, as compared to $\lambda = 0.88$. The effect of the efficiency factor on the spectral function is shown in

the inset of Figure 3, where we also display $F(\omega)$ scaled to emphasize the strikingly similar shape of the phonon density of states and the electron-phonon spectral functions. The ratio of $\alpha^2 F(\omega)$ to $F(\omega)$ gradually increases with frequency at about one third of the rate seen in lead.[2]

Figure 4 shows four electron–phonon coupling functions $\alpha^2 F(\omega)$: The calculated *ab initio* result and three curves extracted from experimental tunneling data. All three extracted curves are based on the same tunneling data taken at $T = 0.35$ K,[17] which should be more accurate than the data taken at higher temperatures.[18] The extracted curves differ in the constraints imposed on their low- and high-frequency behavior. The unconstrained curve is quadratic for $\omega < 0.5$ meV and uses $\omega_{max} = 21$ meV. While this curve yields the best fit to the relative tunneling conductance, it shows what is believed to be unphysical behavior at low and high energies. There is no reason to believe that there is a phonon feature at 1.5 meV as shown in the unconstrained curve. Rather, that shoulder is most likely an artifact related to the accuracy of the voltage (and of Δ_0) for the experimental data collected at low energies. The features at high energy may be real, i.e., structure from either vertex corrections or from interface phonons, but most likely they arise from forcing an accurate fit to the experimental data at approximately 13 meV above the superconducting gap. We estimate that vertex corrections lead to a small reduction of T_C of approximately 0.3%, based on a simple integral of $\alpha^2 F(\omega)$ (using the Fermi-surface average $C = 0.18$).[16] This result is the same size of effect as seen in lead, so vertex corrections can be safely neglected for indium.

The constrained curve is more strongly restricted in its shape at both low- and high-energies: $\alpha^2 F(\omega)$ is forced to increase quadratically in ω for $\omega < 2$ meV and decay linearly to zero at the maximum bulk phonon frequency of 16 meV. These constraints eliminate what appear to be unphysical features in the unconstrained $\alpha^2 F(\omega)$, while still fitting the tunneling data extremely well. The fourth curve shown in Figure 4 is that of Dynes,[17] on which the three-decade-old value for λ is based. His calculation differs from ours in that it was performed directly on the real axis, which does not handle μ^* properly,[28] and it was not performed relative to the normal state, which would enforce the correct energy dependence at high energies.

For each of the $\alpha^2F(\omega)$ shown in Figure 4, the differences between the measured and calculated tunneling conductance are plotted in Figure 5. It is remarkable that an *ab initio* calculation with only one adjustable parameter (the Morel-Anderson pseudopotential μ^*, adjusted to give the superconducting gap at zero temperature) can fit the experimental tunneling conductance to better than one part in 10^3 (the tunneling conductance is on the order of 1). Furthermore, we see that the low- and high-frequency features unique to the unconstrained curve greatly improve the fit only in the low and high energy ranges. Since the experimental data is least accurate in these ranges, it makes sense to constrain the fitting procedure to suppress the unphysical features that stem from these ranges. Ideally, the best way to proceed would be to use experimental data that has error bars reported with it. Such data would allow a maximum entropy technique to be employed to produce the best fit $\alpha^2F(\omega)$.[34]

Table I describes the curves extracted from tunneling data and the *ab initio* calculation. The electron-phonon spectral functions are characterized by several moments:[2] (i) the electron–phonon mass-renormalization parameter λ (twice the first inverse moment), (ii) the strength A (the area under the curve), and (iii) the characteristic phonon energy ω_{ln} (a logarithmic moment). The extracted $\alpha^2F(\omega)$ and Morel-Anderson pseudopotential μ^* (adjusted to reproduce the experimental Δ_0) are employed to calculate the critical temperature T_C with no further adjusting of parameters. All results lie within 5% of the experimental T_C. The errors in the tunneling conductance are all rather close (with exception of the unconstrained curve), whereas the curves differ significantly in their moments.

One possible explanation for the wide variation in the moments is the smallness of λ for indium combined with the experimental uncertainty in the superconducting gap at zero temperature, Δ_0. Since μ^* is adjusted to give Δ_0 and materials with small λ do not display strong features in the tunneling DOS, it is difficult to extract $\alpha^2F(\omega)$ to high accuracy. The value of $\alpha^2F(\omega)$ in the region between 0 and 3 meV has a large effect on the size of the extracted λ, but this is the region where the experimental data depends most on the precise knowledge of Δ_0 and the experimental voltage.

Given the range of λ from 0.8 to 1.1 for the different $\alpha^2F(\omega)$, it is not surprising that μ^* also spans a wide range. Conventional wisdom limits μ^* to the range of 0.1 to 0.14 for

most materials. In fact, this was a criterion used for choosing junctions in the tunneling experiments.[18] However, our *ab initio* $\alpha^2 F(\omega)$ as well as our constrained and unconstrained $\alpha^2 F(\omega)$ extracted from tunneling data all give μ^* larger than the conventional values. Recent first-principles calculations of μ^* suggest that $\mu^* < 0.14$ is an artificial limit for some simple metals.[35] Within the standard Eliashberg theory, where a constant electronic DOS is assumed, $\mu^* = \mu/[1 - \mu \ln(N(E_F) 6\omega_{max})]$, and the maximum value is found by letting μ become infinite. For indium, this gives a maximum μ^* of about 0.25. We get the same estimate for a maximal μ^* by including the energy dependence of the electronic DOS, i.e., the $N(E)$ of Fig. 1, in[36,37]

$$\mu^*_{max} = \frac{\pi N(E_F)}{\int_{-\infty}^{\infty} \frac{dy}{y} N(E_F + y) \left(\tan^{-1}\left(\frac{y}{6\omega_{max}} \right) - \tan^{-1}\left(\frac{y}{\omega_p} \right) \right)}, \tag{5}$$

with a plasma frequency $\omega_p \approx 12$ eV. We expect $\mu < 1$ in indium because it is an *s-p* metal, well described by the free-electron model, so expected values of μ^* should be less than 0.2. All these estimates indicate that the unconstrained curve is unphysical.

Even if we discount the unconstrained curve, the remaining values for λ differ by up to 20%. Low-temperature specific heat data can be used to provide an additional estimate for λ. Using the linear coefficient γ from experiment[38] and our calculated electronic DOS at the Fermi level, we estimate $\lambda = 0.86$, which is close to the *ab initio* value. This estimate is uncertain because the experimental γ itself is known only to a few percent,[38] and furthermore the estimate relies on a precise knowledge of the electronic DOS at the Fermi level and on the assumption that electron–electron effects do not contribute significantly to the mass renormalization. Taken together, these results lead us to conclude that for indium $\lambda = 0.9 \pm 0.1$.

IV. CONCLUSIONS

State-of-the-art *ab initio* methods deliver a very accurate description of the electron–phonon coupling in indium: The calculated relative tunneling conductance agrees with experiment to better than one part in 10^3; the calculated intrinsic resistivity as a function of temperature is also in good agreement with experiment. The achieved accuracy justifies the

approximations invoked: The local density approximation used to calculate the electronic structure and the harmonic approximation for the phonons.

Indium is a good choice for the comparison also because of the high quality experimental tunneling data. Still, we do not know the strength of the electron–phonon mass-renormalization parameter λ as well as it would seem from the literature. Based on our calculations with state-of-the-art many-body theory methods, we estimate that λ can only be determined to within 10%, because of uncertainties in the data at low and high energies. The uncertainties lead to the question of how to best extract the electron–phonon spectral function $\alpha^2 F(\omega)$ from experimental data: Is it better to fit the data as precisely as possible or to allow for experimental errors at low and high energies by constraining the curve to be physically reasonable? All the $\alpha^2 F(\omega)$ — *ab initio*, many-body with and without constraints — show the same structure with roughly the same magnitude. The tunneling conductance obtained from our *ab initio* $\alpha^2 F(\omega)$ is as accurate as the tunneling conductance obtained from the most likely spectral function extracted from the experimental data.

From our study we conclude that the accuracy with which the electron–phonon coupling strength is extracted from experiment could be improved. In particular, we hope to motivate further experimental work that reports error bars for the tunneling conductance and the superconducting gap so that a maximum-entropy technique can be employed to determine the best fit $\alpha^2 F(\omega)$. In materials where vertex corrections are more important, the improved accuracy of $\alpha^2 F(\omega)$ would also allow the effects of vertex corrections to be observed in the multiphonon region.

REFERENCES

[1] G. M. Eliashberg, Zh. Eksperim. i Teor. Fiz. **38**, 966 (1960) [translation: Soviet Phys. – JETP **11**, 696 (1960)].

[2] J. P. Carbotte, Rev. of Mod. Phys. **62**, 1027 (1990).

[3] S. Baroni, P. Giannozzi, and A. Testa, Phys. Rev. Lett. **58**, 1861 (1987).

[4] A. A. Quong and B. M. Klein, Phys. Rev. B **46**, 10734 (1992).

[5] S. Y. Savrasov, Phys. Rev. Lett. **69**, 2819 (1992).

[6] S. Y. Savrasov, D. Y. Savrasov, and O. K. Andersen, Phys. Rev. Lett. **72**, 372 (1994); S. Y. Savrasov and D. Y. Savrasov, Phys. Rev. B **54**, 16487 (1996).

[7] A. Y. Liu and A. A. Quong, Phys. Rev. B **53**, 7575 (1996).

[8] P. K. Lam, M. L. Cohen, Phys. Rev. B **25**, 6139 (1982); P. K. Lam, M. M. Dacorogna, and M. L. Cohen, *ibid.* **34**, 5065 (1986).

[9] S. Wei and M. Y. Chou, Phys. Rev. Lett. **69**, 2799 (1992); Phys. Rev. B **50**, 2221 (1994).

[10] R. Heid, K.-P. Bohnen, and K. M. Ho, Phys. Rev. B **57**, 7407 (1998).

[11] R. Bauer, A. Schmid, P. Pavone, and D. Strauch, Phys. Rev. B **57**, 11276 (1998).

[12] W. L. McMillan and J. M. Rowell, Phys. Rev. Lett. **14**, 108 (1965); in *Superconductivity*, edited by R. Parks (Dekker, New York, 1969), Vol. 1, p. 117.

[13] P. B. Allen, Phys. Rev. B **3**, 305 (1971).

[14] J. R. Schrieffer, D. J. Scalapino, and J. W. Wilkins, Phys. Rev. Lett. **10**, 336 (1963).

[15] E. L. Wolf, *Principles of Electronic Tunneling Spectroscopy* (Oxford University Press, New York, 1985), p. 164.

[16] J. K. Freericks, E. J. Nicol, A. Y. Liu, and A. A. Quong, Phys. Rev. B **55**, 11651 (1997).

[17] J. M. Rowell, W. L. McMillan, and R. C. Dynes (unpublished).

[18] R. C. Dynes, Phys. Rev. B **2**, 644 (1970).

[19] J. Perdew and A. Zunger, Phys. Rev. B **23**, 5048 (1981).

[20] N. Troullier and J. L. Martins, Phys. Rev. B **43**, 8861 (1991).

[21] S. G. Louie, S. Froyen, and M. L. Cohen, Phys. Rev. B **26**, 1738 (1982).

[22] H. J. Monkhorst and J. D. Pack, Phys. Rev. B **13**, 5188 (1976).

[23] M. Methfessel and A. T. Paxton, Phys. Rev. B **40**, 3616 (1989).

[24] G. Lehmann and M. Taut, Status Solidi B **54**, 469 (1972).

[25] P. B. Allen, Phys. Rev. B **6**, 2577 (1972).

[26] P. B. Allen, Phys. Rev. B **17**, 3725 (1978).

[27] F. Marsiglio, M. Schossmann, and J. P. Carbotte, Phys. Rev. B **37**, 4965 (1988).

[28] C. R. Leavens and E. W. Fenton, Solid State Commun. **33**, 597 (1980).

[29] C. S. Owen and D. J. Scalapino, Physica **55**, 691 (1971).

[30] H. G. Smith and W. Reichardt, *Numerical Data and Functional Relationships in Science and Technology*, New Series, Vol. 13a, edited by K.-H. Hellwege and J. L. Olsen, (Springer Verlag, Berlin-Heidelberg, 1981), p. 67.

[31] J. Bass, *Numerical Data and Functional Relationships in Science and Technology*, New Series, Vol. 15a, edited by K.-H. Hellwege and J. L. Olsen, (Springer Verlag, Berlin-Heidelberg, 1981), p. 43.

[32] N. W. Ashcroft and N. D. Mermin, *Solid State Physics* (Saunders, Philadelphia, 1976) p. 461.

[33] F. J. Pinski, P. B. Allen, and W. H. Butler, Phys. Rev. B **23**, 5080 (1981).

[34] M. Jarrell and J. E. Gubarnatis, Phys. Rep. **269**, 133 (1996).

[35] Y. G. Jin and K. J. Chang, private communication.

[36] F. Marsiglio, J. Low Temp. Phys. **87**, 659 (1992).

[37] J. K. Freericks and M. Jarrell, Phys. Rev. Lett. **75**, 2570 (1995).

[38] H. R. O'Neal and N. E. Phillips, Phys. Rev. **137**A, 748 (1965); H. W. White and D. C. Mc-Collum, Phys. Rev. B **1**, 552 (1970).

[39] G. Gladstone, M. A. Jensen, and J. R. Schrieffer, *Superconductivity*, R. D. Parks, ed. (Dekker, New York, 1969) p. 734.

FIGURES

FIG. 1. Electronic density of states from the *ab initio* calculation; inset: density of states near the Fermi level. The *ab initio* results (solid curve) are compared to the free-electron density of states (dashed curve). The inset shows that the calculated density of states changes by only a few percent within the range of $E_F \pm 6\omega_{max}$, where ω_{max} is the maximum phonon frequency; this justifies the assumption of a constant DOS in this region for the many-body-theory calculations.

FIG. 2. Phonon dispersion along the high-symmetry directions shown in the inset. The experimental data and corresponding fit are from Ref. 30. The *ab initio* results are calculated on a uniform grid of 59 **q**-points in the irreducible wedge of the BZ and then interpolated to a denser mesh by means of a Fourier deconvolution.

FIG. 3. Electrical resistivity as a function of temperature. The dashed and solid curves are calculated using the *ab initio* results for the electron-phonon spectral function $\alpha^2 F(\omega)$ and its transport analog $\alpha_{tr}^2 F(\omega)$, respectively. The latter agrees significantly better with the experimental data.[31] The inset shows the strikingly similar shape of the phonon density of states $F(\omega)$, $\alpha^2 F(\omega)$, and $\alpha_{tr}^2 F(\omega)$, with the units scaled to display $F(\omega)$ with a magnitude similar to that of the spectral functions.

FIG. 4. Electron–phonon spectral functions $\alpha^2 F(\omega)$ from *ab initio* calculations and extracted from experimental tunneling results. The three extracted curves are all based on the same tunneling data, but differ in the constraints used in the tunneling inversion procedure. The unconstrained curve shows spurious behavior at low frequencies and above the maximum phonon frequency.

FIG. 5. Differences between the measured and calculated tunneling conductances based on the spectral functions $\alpha^2 F(\omega)$ in Fig. 4. The unconstrained $\alpha^2 F(\omega)$ yields errors in the conductance that are two orders of magnitude smaller than any of the other $\alpha^2 F(\omega)$ curves.

TABLES

| | λ | A (meV) | ω_{ln} (meV) | μ^* | T_C (K) | error in tunneling conductance | |
						max (10^{-3})	rms (10^{-4})
experiment[39]					3.40		
ab initio	0.882	3.00	5.61	0.161	3.31	1.1	6
unconstrained	1.108	3.66	5.20	0.326	3.24	0.04	0.08
constrained	0.984	3.24	5.51	0.224	3.28	2.3	5
Ref. 17	0.805	2.74	5.84	0.119	3.32	0.9	7

TABLE I. Parametric description of the $\alpha^2 F(\omega)$ functions from the *ab initio* calculation and extracted from tunneling data. The electron-phonon spectral functions are characterized by several moments: (i) the electron–phonon mass-renormalization parameter λ (twice the first inverse frequency moment), (ii) the strength A (the area under the curve), and (iii) the characteristic phonon energy ω_{ln} (a logarithmic moment). The Morel-Anderson pseudopotential μ^* is adjusted to reproduce the experimental gap at T=0. Results for the critical temperature T_C, calculated from $\alpha^2 F(\omega)$ and μ^*, all lie within 5% of the experimental T_C. Also listed are the maximum and the RMS errors in the tunneling conductance.
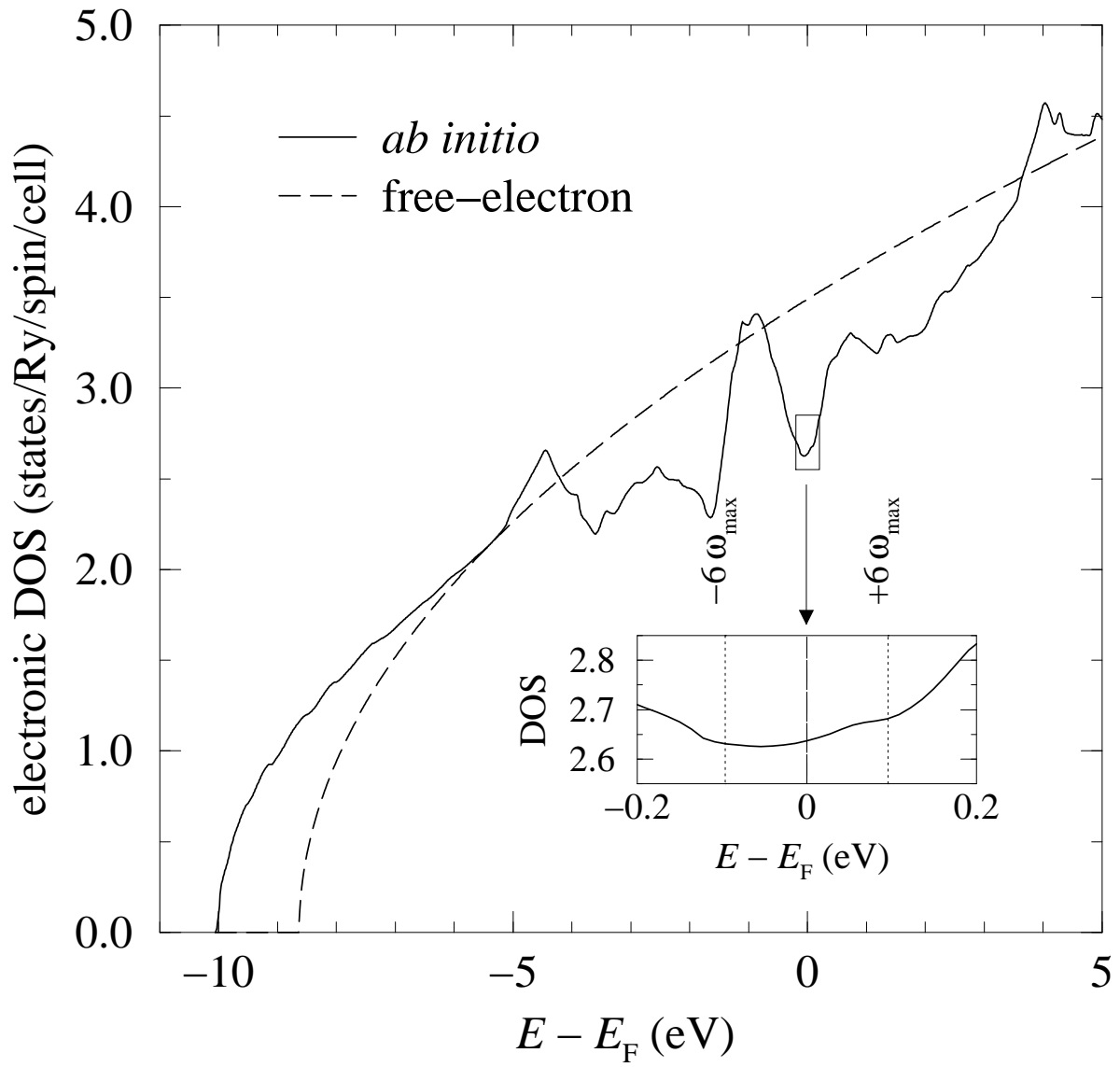
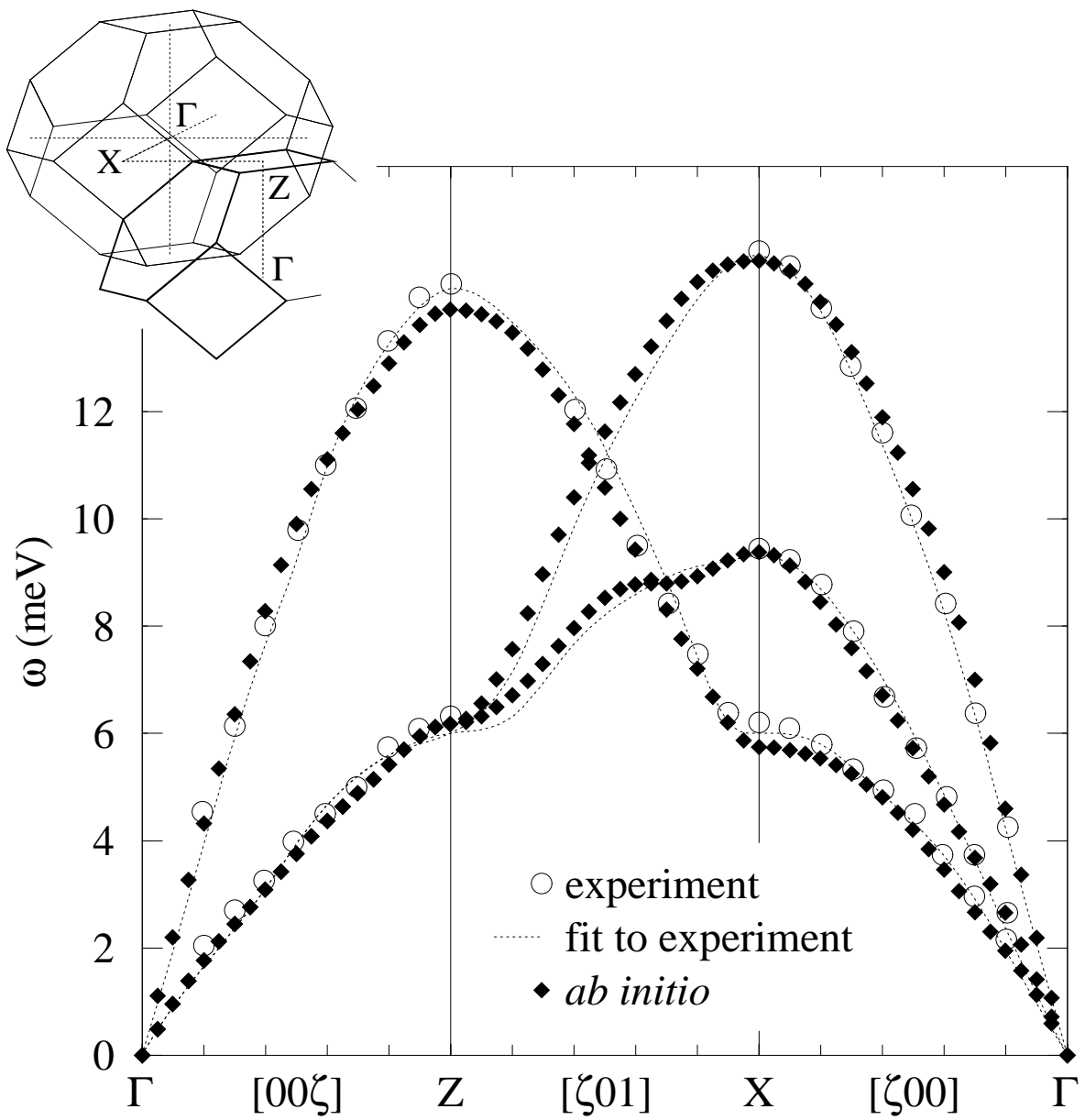Figure 1 — Rudin, Bauer, Liu, Freericks
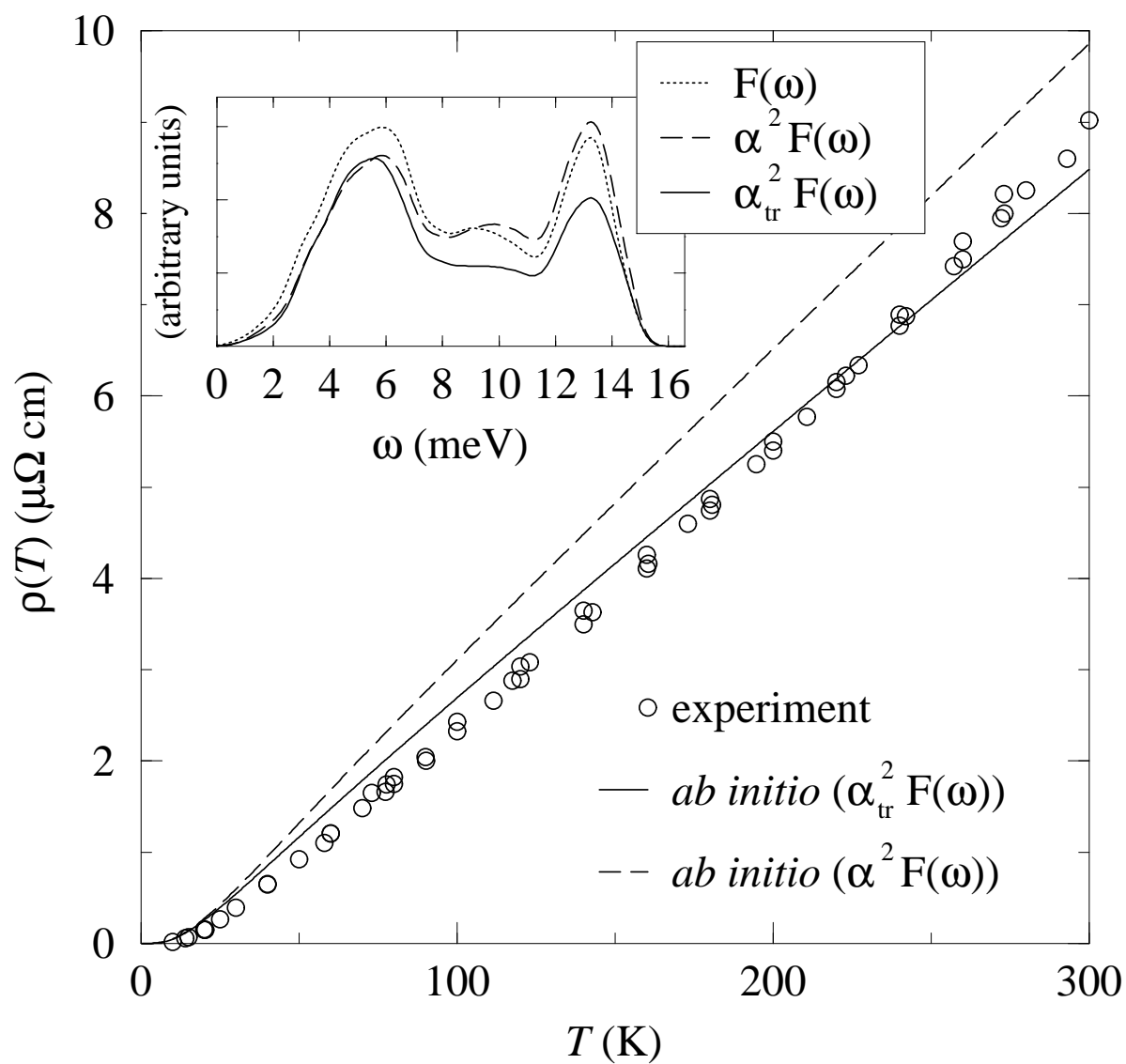
Figure 2 — Rudin, Bauer, Liu, Freericks
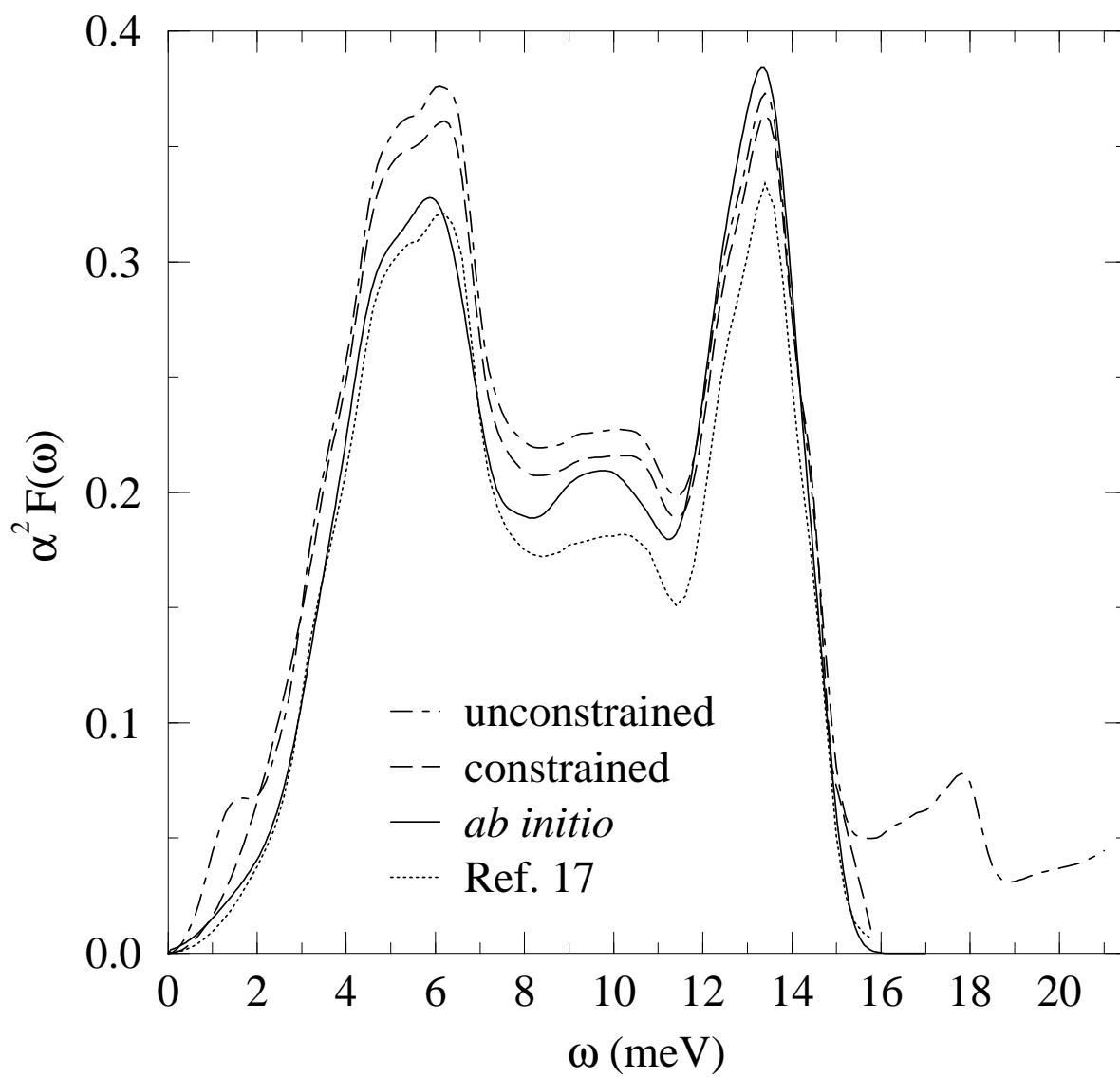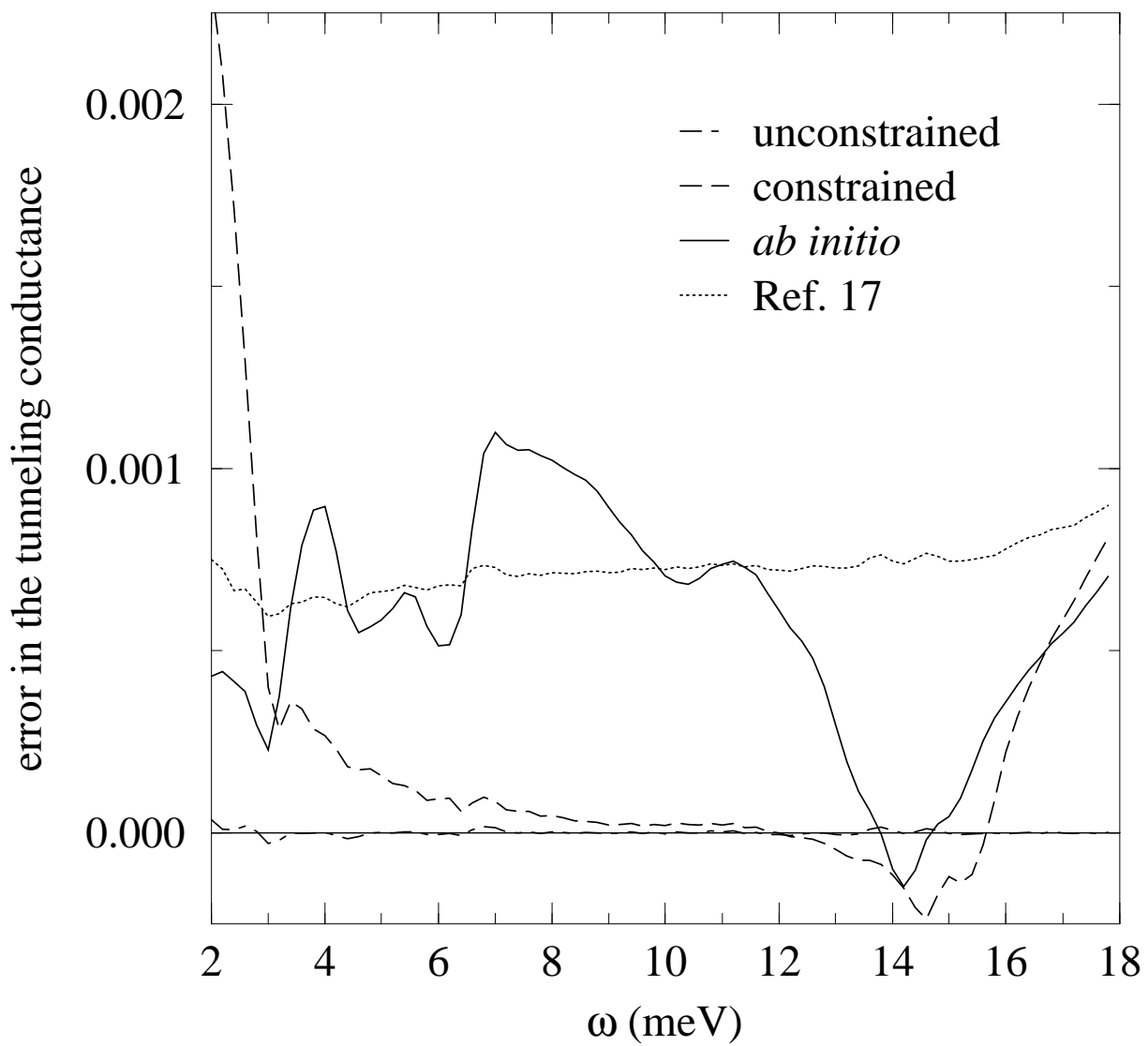
Figure 3 — Rudin, Bauer, Liu, Freericks

Figure 4 — Rudin, Bauer, Liu, Freericks

Figure 5 — Rudin, Bauer, Liu, Freericks